Evaluation of a Mitochondrial Voltage Sensor, (^{18}F-Fluoropentyl)Triphenylphosphonium Cation, in a Rat Myocardial Infarction Model

Dong-Yeon Kim[1,2], Hyeon-Sik Kim[1], Uyenchi Nguyen Le[1], Sheng Nan Jiang[1], Hee-Jung Kim[2], Kyo-Chul Lee[3], Sang-Keun Woo[3], Jihwa Chung[1], Hyung-Seok Kim[4], Hee-Seung Bom[1], Kook-Hyun Yu[2], and Jung-Joon Min[1]

[1]Department of Nuclear Medicine, Chonnam National University Medical School, Gwangju, Republic of Korea; [2]Department of Chemistry, Dongguk University-Seoul, Seoul, Republic of Korea; [3]Molecular Imaging Research Center, Korea Institute of Radiological and Medical Sciences, Seoul, Republic of Korea; and [4]Department of Forensic Medicine, Chonnam National University Medical School, Gwangju, Republic of Korea

Radiolabeled lipophilic cationic compounds, such as ^{18}F-labeled phosphonium salt, accumulate in the mitochondria through a negative inner transmembrane potential. The purpose of this study was to develop and evaluate (^{18}F-fluoropentyl)triphenylphosphonium salt (^{18}F-FPTP) as a myocardial PET agent. **Methods:** A reference compound of ^{18}F-FPTP was synthesized via 3-step nucleophilic substitution reactions and was radiolabeled via 2-step nucleophilic substitution reactions of no-carrier-added ^{18}F-fluoride. Accumulations of ^{18}F-FPTP, ^{3}H-tetraphenylphosphonium, and ^{99m}Tc-sestamibi were compared in a cultured embryonic cardiomyoblast cell line (H9c2). The biodistribution of ^{18}F-FPTP was assessed using BALB/c mice. The ^{18}F-FPTP small-animal PET study was performed in Sprague–Dawley rats with or without left coronary artery (LCA) ligation. **Results:** ^{18}F-FPTP was synthesized with a radiochemical yield of 15%–20% and radiochemical purity of greater than 98%. Specific activity was greater than 6.3 TBq/μmol. Cell uptake of ^{18}F-FPTP was more than 15-fold higher in H9c2 than in normal fibroblasts (human normal foreskin fibroblasts). Selective collapse of mitochondrial membrane potential substantially decreased cellular uptake for ^{18}F-FPTP and ^{3}H-tetraphenylphosphonium, compared with that for ^{99m}Tc-sestamibi. The biodistribution data in mice (n = 24) showed rapid blood clearance and high accumulation in the heart. Heart-to-blood ratios at 10 and 30 min were 54 and 133, respectively. Heart-to-lung and heart-to-liver ratios at 10, 30, and 60 min were 4, 4, and 7 and 4, 5, and 7, respectively. Dynamic small-animal PET for 60 min after injection of ^{18}F-FPTP showed an initial spike of radioactivity, followed by retention in the myocardium and rapid clearance from the background. ^{18}F-FPTP small-animal PET images in LCA-occluded rats demonstrated sharply defined myocardial defects in the corresponding area of the myocardium. The myocardial defect size measured by ^{18}F-FPTP small-animal PET correlated closely with the hypoperfused area measured by quantitative 2,3,5-triphenyltetrazolium chloride staining (r^2 = 0.92, $P < 0.001$). **Conclusion:** The excellent pharmacokinetics of ^{18}F-FPTP and its correlation with 2,3,5-triphenyltetrazolium chloride staining in normal and LCA-occluded rats suggest that this molecular probe may have a high potential as a mitochondrial voltage sensor for PET. This probe may also allow high throughput, with multiple daily studies and a wide distribution of PET myocardial imaging in the clinic.

Key Words: mitochondrial membrane potential; myocardial imaging agent; ^{18}F-labeled phosphonium salt; positron emission tomography (PET); myocardial infarction

J Nucl Med 2012; 53:1779–1785
DOI: 10.2967/jnumed.111.102657

Nuclear medicine technologies using SPECT play a key role in the diagnosis of coronary artery disease. SPECT agents such as ^{201}Tl, ^{99m}Tc-sestamibi, and ^{99m}Tc-tetrofosmin are the mainstay of myocardial perfusion imaging tests (*1*). However, the absence of a standardized method of SPECT for the correction of photon attenuation and the suboptimal spread of SPECT tracers in organs adjacent to the heart may lead to artifact formation, which can interfere with the detection of flow abnormalities (*2*). PET has several technical advantages over SPECT, such as a higher spatial resolution. Because of accurate attenuation correction, it can provide quantitative measures of myocardial tracer uptake (*3*). However, the short half-life of currently used PET tracers for myocardial imaging (e.g., ^{13}N-ammonia, ^{82}Rb, and ^{15}O-water) limits the widespread clinical use of PET because of the need for a nearby cyclotron or generator (*4,5*). ^{18}F-labeled myocardial imaging tracers, with their longer half-life and better spatial resolution, would avoid these limitations and facilitate clinical protocols (*6,7*).

To address this need, several previous publications have reported ^{18}F-labeled phosphonium cations (*2,8–12*). Similar to SPECT tracers such as ^{99m}Tc-sestamibi and ^{99m}Tc-tetrofosmin, phosphonium cations accumulate to a higher degree in

Received Jan. 5, 2012; revision accepted Jun. 5, 2012.
For correspondence or reprints contact either of the following: Jung-Joon Min, Department of Nuclear Medicine, Chonnam National University Medical School, 160 Ilsimri, Hwasun, Jeonnam 519-763, Gwangju, Republic of Korea.
E-mail: jjmin@jnu.ac.kr
Kook-Hyun Yu, Department of Chemistry, Dongguk University-Seoul, 30 Pildong-ro 1-Gil, Jung-gu, Seoul, 100-715, Republic of Korea.
E-mail: yukook@dongguk.edu
Published online Oct. 4, 2012.

cardiomyocytes than in normal cells because of the higher mitochondrial membrane potential (MMP) in cardiomyocytes (*10,13–17*). This type of mitochondrial voltage sensor would be useful to detect myocardial abnormalities because loss of MMP is an early event in cell death caused by myocardial ischemia (*10,17–19*). Moreover, cumulative evidence suggests that mitochondria-controlled apoptosis underlies cell loss in heart failure (*20*). ^{18}F-fluorobenzyl triphenylphosphonium (^{18}F-FBnTP) was the first ^{18}F-labeled phosphonium cation that has been actively investigated, and it has demonstrated excellent characteristics as a cardiac imaging agent in both healthy and coronary artery disease models (*2,10,14*).

Herein, we report the synthesis and characterization of an ^{18}F-labeled phosphonium cation, (^{18}F-fluoropentyl)triphenylphosphonium salt (^{18}F-FPTP), as a voltage sensor for myocardial imaging (*8,9,11*). Biologic studies, such as a biodistribution study and small-animal PET in rat models, demonstrated intense initial myocardial uptake with rapid clearance from the background, possibly allowing high throughput with multiple daily studies in the clinic.

MATERIALS AND METHODS

Full details of all methods and equipments are presented in the supplemental materials (available online only at http://jnm.snmjournals.org).

Radiochemistry

^{18}F-fluoride was produced by an ^{18}O(p,n)^{18}F reaction on a PET-trace cyclotron (GE Healthcare). Activity was extracted from $H_2{}^{18}O$ by an anion exchanger and then eluted by aqueous potassium carbonate (25.0 mmol) into the reaction vessel. The radioactive solution was dried together with 4.0 mg of Kryptofix 2.2.2 (Sigma-Aldrich) in 1.0 mL of acetonitrile under nitrogen at 100°C. The solution was evaporated at 100°C by bubbling nitrogen gas, and the residue was dried by azeotropic distillation with acetonitrile (1 mL, 3 times). Next, 4.0 mg of pentane-1,5-diyl bis(4-methylbenzenesulfonate) dissolved in 1.0 mL of anhydrous acetonitrile were added. Pentane-1,5-diyl bis(4-methylbenzenesulfonate) was prepared by modification of a previously reported method (*21*). The mixture was heated for 5 min at 90°C in the closed state. Radio–thin-layer chromatography showed a yield of more than 80% of the compound ^{18}F-fluoropentyl 4-methylbenzenesulfonate. The solution was passed through a small silica Sep-Pak cartridge (Waters). Triphenylphosphine (6.0 mg) was dissolved in 1.0 mL of toluene, added to the reaction vessel, and heated to 220°C for 3 min with no separation step (Fig. 1) (*22*).

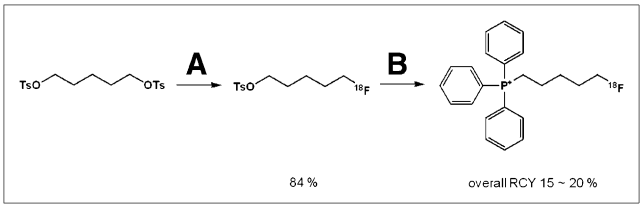

FIGURE 1. Radiosynthesis of (5-fluoropentyl)triphenylphosphonium salt. Reagents and conditions were as follows: (A) ^{18}F-KF, acetonitrile, Kryptofix 2.2.2, 90°C, 5 min; (B) triphenylphosphine, toluene, 220°C, 3 min. RCY = radiochemical yield.

The solution was cooled and injected onto a semipreparative high-performance liquid chromatography (HPLC) column system for purification (acetonitrile:phosphate-buffered saline (PBS), 45:55; flow rate, 3 mL/min; ultraviolet, 254 nm; retention time, 21.8 min). For identification of the radioproduct, the collected HPLC fraction was coinjected with its nonradioactive compound. ^{18}F-FPTP was dried, made isotonic with sodium chloride, and passed through a 0.20-μm membrane filter into a sterile multidose vial for in vitro and in vivo experiments.

Partition Coefficient and Stability Study

The log P was measured to compare the lipophilicities of ^{18}F-FPTP, ^{3}H-tetraphenylphosphonium (Moravek Biochemicals, Inc.), and ^{99m}Tc-sestamibi. After the complete removal of volatiles of ^{18}F-FPTP, ^{99m}Tc-sestamibi and the residues were dissolved in a mixture of 3 mL of saline and 3 mL of *n*-octanol in a round-bottom flask. The mixture was vigorously stirred for 20 min at room temperature and was transferred to 15-mL Falcon conical tubes. The tubes were centrifuged at 3,000 rpm for 5 min. Samples in triplicate from *n*-octanol and aqueous layers were obtained and counted on a γ-counter (*23*). The partition coefficient of ^{3}H-tetraphenylphosphonium was measured in the same manner and was counted on a liquid scintillation counter. The log P value was reported as the average of data obtained in 3 independent measurements (*24*).

For the labeling stability test, ^{18}F-FPTP (0.37 MBq/100 μL) was incubated with human serum (1.0 mL) at 37°C in a water bath for 4 h and then analyzed by chromatography on instant thin-layer chromatography silica gel strips developed with a 9:2 ratio of methylene chloride:methanol. After they were developed, the chromatographic strips were scanned on an automatic thin-layer chromatography device. Thin-layer chromatography was performed at various time points. All experiments were done in triplicate (*25*). Also, for in vivo stability evaluation, 3 BALB/c mice (weight, 18–20 g; Orient) were used. After intravenous injection of ^{18}F-FPTP (7.4 MBq), the mouse blood was collected at each time point (10, 30, 60, 120, and 240 min). The collected mouse serum was filtered and analyzed by HPLC.

Cell Lines, Culture Conditions, and Cell Uptake Studies

^{18}F-FPTP accumulation was measured in cell culture with a rat embryonic cardiomyoblast cell line (H9c2). Human normal foreskin fibroblasts (HDFs) were used as a negative control. All cells were grown in deficient Dulbecco modified Eagle medium high glucose (containing 5.3 mM KCl and 110.34 mM NaCl; Life Technologies) plus 5% fetal bovine serum, 1% penicillin-streptomycin, and 1% L-glutamine. For the uptake test, cells were incubated at 37°C for 60 min with serum-free, radioactive culture medium. Radioactivity was measured after radioactive medium was removed. The wells were washed 3 times with cold PBS. The cells were harvested, and the cell-associated radioactivity was determined. The MMP-dependent cellular uptake of ^{18}F-FPTP, ^{3}H-tetraphenylphosphonium, and ^{99m}Tc-sestamibi was assessed with H9c2 cells treated with carbonyl cyanide *m*-chlorophenylhydrazone (CCCP), which is a protonophore that selectively abolishes the MMP (*26*). The compound was dissolved in dimethyl sulfoxide and diluted to the desired concentration with low K^+ *N*-(2-hydroxyethyl)piperazine-*N*′-(2-ethanesulfonic acid) (HEPES) buffer. The final concentrations of dimethyl sulfoxide were less than 0.1%. Different concentrations of CCCP solution (0.10, 0.50, 1.0, and 10.00 μM) were added to 5.0×10^4 cells at 30 min before the start of the experiment.

Radioactivity was determined by γ-counter or liquid scintillation counter after 1 h of incubation with ^{18}F-FPTP, ^{3}H-tetraphenylphosphonium, or ^{99m}Tc-sestamibi (*27*). Triplicate samples were obtained for all uptake studies, and data are expressed as the net accumulation of probe, in (dpm cells/dpm medium/μg total protein) ± SE.

Animal Model and Murine Biodistribution Studies

Eight-week old male Sprague–Dawley rats (weight, 250–260 g; Orient) underwent left coronary artery (LCA) ligation, as previously described (*28*). Animal care, all experiments, and euthanasia were performed in accordance with protocols approved by the Chonnam National University Animal Research Committee and the *Guide for the Care and Use of Laboratory Animals* published by the National Institutes of Health (*29*). Animals underwent imaging studies at 24 h after LCA occlusion.

To confirm the activity of ^{18}F-FPTP in vivo, biodistribution studies were performed with murine models. Biodistribution in different organs was assessed in BALB/c mice at 10, 30, 60, and 120 min after intravenous injection of 7.4 MBq of radiotracer ($n = 6$, each). Blood, heart, lung, liver, spleen, stomach, intestine, kidney, pancreas, muscle, and bone were sampled from the mice, and the radioactivity of each organ was measured with a γ-counter. Radioactivity determinations were normalized by the weight of the tissue and the amount of radioactivity injected to obtain the percentage injected dose per gram (%ID/g).

Small-Animal PET and Quantitative Analysis

A dedicated small-animal PET/CT scanner (Inveon; Siemens Medical Solutions) was used for in vivo imaging of ^{18}F-FPTP kinetics. Normal or myocardial infarction (MI) rats were anesthetized with isoflurane, placed in a cradle, and equipped with masks for anesthesia gas supply and warm water pads at the tail veins for injection. Dynamic small-animal PET images were acquired for 60 min (40 s × 15 frames, 100 s × 30 frames) after injection of ^{18}F-FPTP (37 MBq).

To determine pharmacokinetics, a region of interest was drawn around the heart. Time–activity curves of ^{18}F-FPTP were generated to obtain the counts per pixel per second. Images obtained between 10 and 20 min after tracer injection were reconstructed using the 3-dimensional ordered-subset expectation maximization algorithm with 4 iterations. Reconstructed pixel sizes were 0.78 mm in both the transverse and the axial directions. The dimensions of the reconstructed images were 128 × 128 in each of the 159 transverse slices. Data were normalized and corrected for randoms, dead time, and decay.

Analysis of the small-animal PET images was performed with the PMOD software package (PMOD Technologies Ltd.) (*4,30,31*). To measure the average defect size, reconstructed PET data were reoriented into 20 segments of polar map images. Each polar map was normalized to its maximum. The defect area, which was defined as the fraction of polar map elements with reduced tracer uptake for more than 60% of the maximum, was expressed as the percentage of the left ventricular myocardium.

We compared the defect size on small-animal PET images with the gold standard 2,3,5-triphenyltetrazolium chloride (TTC)–stained images (*32,33*). In the presence of dehydrogenase enzyme that exists in viable myocardium, TTC is reduced and forms a formazan precipitate that makes viable tissue turn brick-red, whereas nonviable infarcted tissue without dehydrogenase activity remains pale. Staining was performed immediately after imaging to avoid further progression of MI. After the rats ($n = 12$) were euthanized, hearts were extracted and washed with 1× PBS. Each heart was frozen and divided perpendicularly into 4–5 cross sections of 1-mm thickness. These sections were incubated for 20 min with a solution of 1% TTC dissolved in 1×PBS at 37°C. Stained sections were washed twice with PBS and stored in 10% formaldehyde for 20 min. Specimens were imaged by a digital camera or placed between 2 glass slides and scanned. The size of the infarcted area (nonstained, pale white region) was measured on both sides, averaged for each slice, and summed from all slices using image processing software (ImageJ, http://rsb.info.nih.gov/ij/).

Statistical Analysis

Comparisons between 2 groups were made with a Student *t* test for independent samples with unequal variances. Comparisons among 3 groups were made with a 1-way ANOVA. *P* values of less than 0.05 were considered statistically significant. Correlation between infarct size measured using small-animal PET and TTC staining was calculated with a Pearson test (2-tailed, 95% confidence interval) using SPSS software (version 18.0; SPSS Inc.).

RESULTS

Radiosynthesis of ^{18}F-FPTP

The scheme for the synthesis of FPTP is shown in Supplemental Figure 1. The reference compound was synthesized via 3-step procedures. All compounds were analyzed by ^{1}H, ^{13}C nuclear magnetic resonance (NMR) spectroscopy, and fast atom bombardment (FAB) or electrospray ionization (ESI) high-resolution mass spectroscopy to confirm the identity. We confirmed the doublet of triplets as characteristic peaks of a fluorine compound in ^{1}H-NMR analysis. The theoretic J value of -CH-F is about 50 Hz; we confirmed that the J values of the fluorine compounds were 47.2 and 47.6 Hz, respectively. We also confirmed 4-methylbenzenesulfonate as a counter ion by ^{1}H-NMR.

The scheme for the radiosynthesis of ^{18}F-FPTP is shown in Figure 1. The analytic HPLC results revealed a single peak, suggesting the formation of 1 product (^{18}F-FPTP) identical to the reference compound. The total reaction time of ^{18}F-FPTP was within 60 min, and the overall decay-corrected radiochemical yield was approximately 15%–20%. Radiochemical purity was greater than 98% based on the analytic HPLC system (same isocratic as used for semipreparative HPLC system; flow rate, 1.0 mL/min; ultraviolet, 254 nm; retention time, 28.9 min). Specific activity was greater than 6.3 TBq/μmol.

To determine the lipophilicity of ^{18}F-FPTP, we assessed the log P values of ^{18}F-FPTP, ^{3}H-tetraphenylphosphonium, and ^{99m}Tc-sestamibi (1.31 ± 0.02, 1.84 ± 0.01, and 0.86 ± 0.01, respectively). When the radiotracer was incubated in human serum at 37°C for 4 h, the percentage of the remaining ^{18}F-FPTP (R_f, 0.45–0.50) was greater than 95%, indicating a relatively high in vitro stability of the radiotracer. No metabolite was detected in the serum of mice after 10 and 30 min of intravenous injection of ^{18}F-FPTP (97.51% ± 4.31% and 96.23% ± 3.31%, respectively).

MMP-Dependent Uptake of ^{18}F-FPTP

The MMP of H9c2 cells, which was assessed by a cellular ^{3}H-tetraphenylphosphonium-uptake assay, was significantly higher than that of HDF cells (Fig. 2A). The uptake of ^{18}F-FPTP was more than 15-fold higher in H9c2 than in HDF

cells (0.0069 ± 0.0004 vs. 0.00046 ± 0.00003, net accumulation of probe [dpm cells/dpm medium/μg total protein ± SE]), consistent with the cell uptake of ^{3}H-tetraphenylphosphonium ($P < 0.01$).

The effects of manipulating MMP on cellular accumulations of ^{18}F-FPTP, ^{3}H-tetraphenylphosphonium, and ^{99m}Tc-sestamibi were assessed through uptake studies on H9c2 cells using 4 concentrations of CCCP (0.1, 0.5, 1.0, and 10 μmol/L) in low-K^+ HEPES buffer. For control experiments in which the MMPs were unaltered, uptake was determined in a near-physiologic buffer (low-K^+ HEPES buffer) without the addition of inhibitors. The uptake of ^{18}F-FPTP in H9c2 cells was significantly inhibited ($P < 0.05$) by CCCP at 1.0 μmol/L, which was comparable to the uptake of ^{3}H-tetraphenylphosphonium. ^{18}F-FPTP uptake was inhibited strongly, to about 25.42% ± 1.16%, by 10 μM CCCP, whereas with ^{99m}Tc-sestamibi, the decrease was less (~48.30% ± 3.20%). Overall, these results clearly demonstrate that ^{18}F-FPTP uptake was electrogenic and MMP-driven.

Biodistribution Study

In vivo biodistribution of ^{18}F-FPTP was examined in BALB/c mice at 10, 30, 60, and 120 min after intravenous injection of ^{18}F-FPTP. A high level of radioactivity accumulation in the heart was observed. The myocardial uptake of ^{18}F-FPTP was more than 20 %ID/g at 10 min of radiotracer injection (Table 1). The heart-to-blood ratio of ^{18}F-FPTP was approximately 54 at 10 min, indicating a rapid clearance of the compound from the blood. The heart-to-lung, heart-to-liver, and heart-to-muscle ratios were >4, >4, and >3, respectively, at 10 min after radiotracer injection. Notably, the heart-to-blood and heart-to-liver ratios increased to more than 550 and more than 10, respectively, at 120 min after radiotracer injection, indicating that ^{18}F-FPTP is optimal as a cardiac imaging agent.

Small-Animal PET and Comparison of MI Size

Dynamic small-animal PET images of rats for 60 min after intravenous injection of ^{18}F-FPTP are shown in Figure 3A and Supplemental Video 1. Good visualization of the heart was obtained, with excellent heart-to-background contrast at each time point. Time–activity curves for the myocardium, liver, and lung revealed rapid washout from the liver and lung after intravenous injection of ^{18}F-FPTP. However, ^{18}F-FPTP was retained at a constant level in the myocardium for up to 1.0 h after injection (Fig. 3B). The myocardium-to-liver and myocardium-to-lung uptake ratios quickly reached 5.0 after ^{18}F-FPTP injection.

Representative images of a rat in the short-, vertical long-, and horizontal long-axes collected between 10 and 20 min after ^{18}F-FPTP injection are shown in Figure 4. In the nonoperative rat, PET demonstrated intense, homogeneous uptake of ^{18}F-FPTP through the left ventricular myocardium (Fig. 4A). In contrast, LCA ligation caused a well-delineated myocardial defect in the anterolateral wall of the left ventricle (Fig. 4B).

The defect size determined by ^{18}F-FPTP small-animal PET showed an excellent correlation with MI size determined by TTC staining (Fig. 5A). The size of the unstained region on the TTC data was compared with the defect size calculated from polar map images. The correlation was excellent ($r^2 = 0.92$, $P < 0.001$) with the 60 threshold in the polar map image (Fig. 5B).

DISCUSSION

^{18}F-FPTP is a derivative of a class of potentiometric lipophilic phosphonium cations that was originally developed for MMP measurement. The lipophilic nature and delocalized positive charge enable the cation to cross the lipid bilayer by passive diffusion and accumulate in cells in a membrane potential–dependent manner (*15,16,34*). Our study demonstrated the possibility of using ^{18}F-FPTP as a myocardial imaging agent targeting the MMP for the evaluation of MI by small-animal PET in rats. This finding is attributed to the higher density and electrochemical membrane potential of the mitochondria in cardiomyocytes (*13,14,24*).

The cellular uptake studies of ^{18}F-FPTP and ^{3}H-tetraphenylphosphonium showed similar values. The results shown in Figure 2A demonstrate that ^{18}F-FPTP was taken up by H9c2 cells at more than 95% of the level at which ^{3}H-tetraphenylphosphonium was taken up (0.0069 and 0.0072, respectively) during their plateau after 60 min of incubation. This information is of particular value for developing ^{18}F-labeled phosphonium cation derivatives as molecular probes for cardiac imaging. We previously demonstrated that ^{3}H-tetraphenylphosphonium accumulates specifically in the

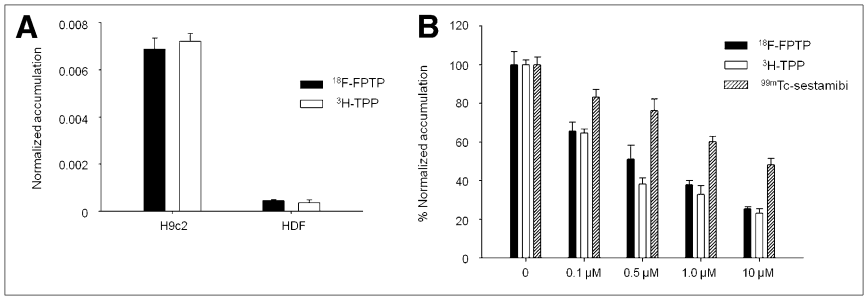

FIGURE 2. (A) Cell uptake study of ^{18}F-FPTP and ^{3}H-tetraphenylphosphonium in H9c2 and HDF cells 60 min after exposure. Uptake of ^{18}F-FPTP was more than 15-fold higher in H9c2 than in HDF cells, consistent with cellular uptake of ^{3}H-tetraphenylphosphonium ($P < 0.01$). Data are expressed as net accumulation of probe in (dpm cells/dpm medium/μg total protein) ± SE. (B) Effect of alteration in MMP on ^{18}F-FPTP, ^{3}H-tetraphenylphosphonium, and ^{99m}Tc-sestamibi cellular uptake. Dose-dependent selective loss of MMP using uncoupler CCCP resulted in more significant decrease of ^{18}F-FPTP and ^{3}H-tetraphenylphosphonium cellular uptake than that of ^{99m}Tc-sestamibi ($P < 0.05$). Values are expressed as mean percentage net accumulation ± SD. TPP = tetraphenylphosphonium.

TABLE 1
Normal Biodistribution Studies in BALB/c Mice at 10, 30, 60, and 120 Minutes After Intravenous Injection of ^{18}F-FPTP

Organ	10 min	30 min	60 min	120 min
Blood	0.39 ± 0.08	0.18 ± 0.02	0.04 ± 0.01	0.04 ± 0.02
Heart	20.57 ± 2.81	23.82 ± 3.23	21.23 ± 3.60	23.04 ± 3.68
Lung	4.96 ± 1.04	4.91 ± 1.05	2.96 ± 0.63	2.98 ± 0.27
Liver	4.81 ± 1.40	4.76 ± 1.06	3.05 ± 0.92	2.15 ± 0.46
Spleen	1.82 ± 0.53	1.79 ± 0.30	1.42 ± 0.44	1.09 ± 0.20
Stomach	4.51 ± 1.38	4.69 ± 1.26	4.34 ± 1.24	3.99 ± 0.91
Intestine	8.45 ± 1.92	11.33 ± 2.70	9.25 ± 5.65	3.69 ± 2.05
Kidney	25.65 ± 6.66	14.25 ± 4.36	11.68 ± 3.73	6.35 ± 2.59
Pancreas	7.33 ± 1.35	8.06 ± 3.73	7.46 ± 1.40	5.53 ± 1.29
Normal muscle	6.18 ± 2.22	6.62 ± 1.36	6.16 ± 1.78	6.06 ± 0.93
Bone	1.89 ± 0.63	1.79 ± 0.62	1.70 ± 0.71	1.57 ± 0.68
Heart to liver	4.46 ± 0.95	5.16 ± 0.98	7.25 ± 1.44	10.72 ± 2.17
Heart to lung	4.21 ± 0.47	4.94 ± 0.67	7.28 ± 1.07	7.72 ± 1.09
Heart to muscle	3.73 ± 1.51	3.69 ± 0.74	3.55 ± 0.48	3.80 ± 0.82
Heart to blood	54.10 ± 13.91	133.49 ± 10.45	523.34 ± 31.41	553.01 ± 23.59

Data are expressed as %ID/g (n = 24). Myocardial uptake of ^{18}F-FPTP was >20 %ID/g at 10 min after radiotracer injection. Heart-to-blood ratio of ^{18}F-FPTP was >54, and heart-to-lung and heart-to-liver ratios were >4 and >4, respectively, at 10 min.

myocardium and tumors, but minimally at inflammatory sites, because of its mitochondria-targeting property (*13*). Cellular uptake profiles using the MMP-modulated cells verified that ^{18}F-FPTP preserved the MMP-dependence property in a manner similar to ^{3}H-tetraphenylphosphonium (*26*) and far better than ^{99m}Tc-sestamibi in cell culture (Fig. 2B). Considering the preferential uptake of ^{18}F-FPTP in embryonic cardiomyoblasts and its higher MMP dependency than ^{99m}Tc-sestamibi, ^{18}F-FPTP is well justified as a molecular probe for mitochondrial voltage imaging.

^{18}F-FPTP biodistribution and PET studies in mice or rats indicated a rapid accumulation of activity in the heart (1–2 min), with stable retention for at least 2 h. Blood washout and hepatic clearance were fast and showed high heart-to-blood ratios (523:1) and favorable heart-to-liver (7:1) and heart-to-lung (7:1) ratios. On the basis of the time–activity curve of small-animal PET images, heart-to-liver and heart-to-lung ratios exceeded 3.0 and 5.0, respectively, within 10 min of injection. These results produced extremely high-quality myocardial images.

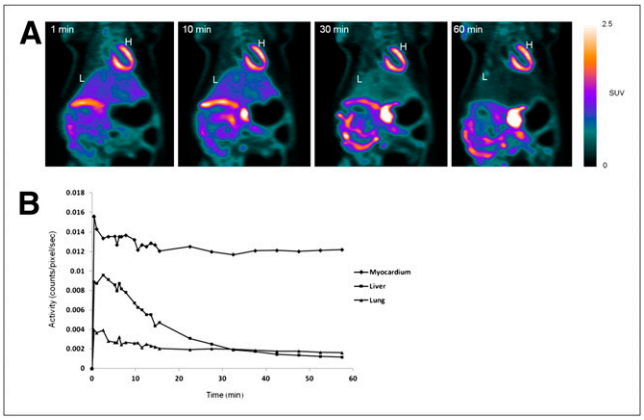

FIGURE 3. (A) Coronal small-animal PET images of rats at 1, 10, 30, and 60 min after intravenous injection of 37 MBq of ^{18}F-FPTP. Heart was visible, with excellent heart-to-background contrast at each time point after tracer injection. (B) Time–activity curves generated from dynamic small-animal PET images for 60 min. ^{18}F-FPTP was retained at constant level in myocardium but was rapidly washed out from liver and lung. *x*-axis shows activity (counts/pixel/s), and *y*-axis shows time (min). H = heart; L = liver; SUV = standardized uptake value.

An important reason for the reduced sensitivity of myocardial imaging is artifacts introduced by suboptimal tracer distribution in organs adjacent to the myocardium. Intense liver uptake, caused by prominent hepatobiliary excretion, is frequently observed on ^{99m}Tc-based myocardial imaging (*35–37*). High liver uptake would result in photon scatter that could mask the detection of flow abnormalities, particularly in the inferior and inferoapical left ventricular wall (*37,38*). The clinically important ratio of ^{18}F-FPTP between myocardium and liver seemed to be higher than that obtained with a recently introduced ^{18}F-labeled phosphonium cation, ^{18}F-FBnTP (7.0 vs. 1.5), in mouse models (*10*). A direct comparison between these 2 tracers will be necessary to ascertain which one has a more favorable biodistribution.

Small-animal PET studies using ^{18}F-FPTP showed an excellent image quality that provided a sharp delineation of myocardial defects produced by acute ligation of the LCA. In the repetitive imaging studies, we uniformly found good image quality that allowed a clear delineation of the borders of the defects. Using polar maps with a 60% threshold, which has the best statistical significance (Supplemental Fig. 8), we found an excellent match of the small-animal PET defect size and the true MI size as measured with TTC staining, which is a gold standard method for measuring the size of both reperfused and nonreperfused MI (Fig. 5). The strong correlation demonstrated that the noninvasive imaging results obtained by ^{18}F-FPTP small-animal PET can serve as a surrogate for the quantification of the infarct size.

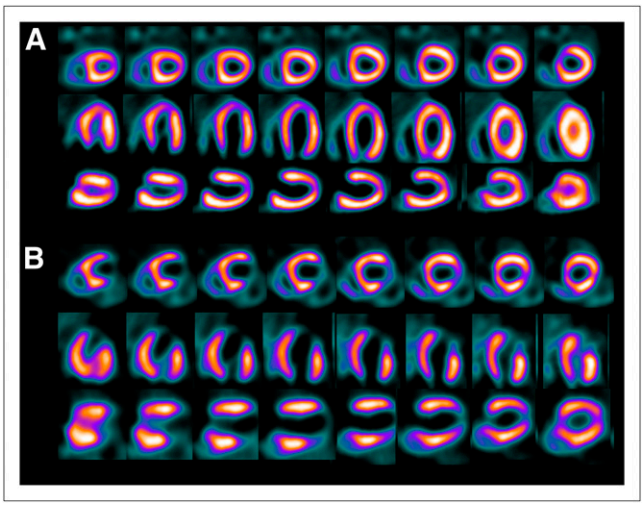

FIGURE 4. Short-, vertical long-, and horizontal long-axis images in normal (A) and LCA-occluded (B) rats. Data were collected between 10 and 20 min after ^{18}F-FPTP injection (37 MBq). Uniform uptake was observed in myocardium of normal rats, whereas sharply defined myocardial deficits were present in LCA-occluded rats.

The rationale for preparing the 5-carbon spacer group was to decrease lipophilicity. Previous publications have reported that ^{18}F-FBnTP is metabolically stable and demonstrates excellent characteristics as a cardiac imaging agent in healthy mice (*10*). However, the myocardium–to–liver uptake ratio in the time–activity curve reached 1.0 at approximately 25 min after intravenous injection of ^{18}F-FBnTP, indicating delayed washout from the liver. Clearance of the radiotracer from the liver is dependent on the lipophilicity of the compound. Thus, in the current study, several kinds of (^{18}F-fluoroalkyl)triphenylphosphonium were synthesized to assess the appropriate lipophilicity by different carbon chain lengths; however, highly lipophilic structures (such as benzene rings) were not adopted for the radiolabeling of phosphonium salts. Compared with ^{18}F-FPTP, the (^{18}F-fluoropropyl)triphenylphosphonium cation (*22*) (a shorter-chain analog) showed a lower myocardial uptake, whereas the (^{18}F-fluorooctyl)triphenylphosphonium cation (a longer-chain analog) showed a higher liver uptake and delayed clearance (data not shown).

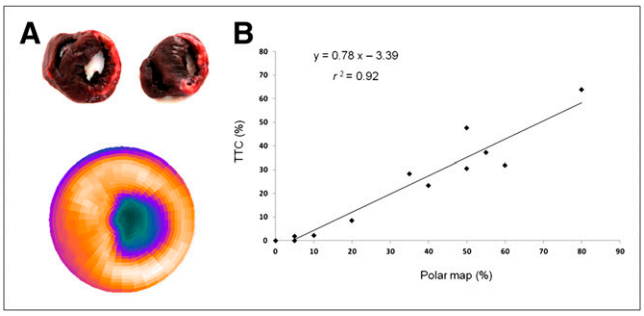

FIGURE 5. (A) Polar map image of ^{18}F-FPTP and corresponding myocardial slices stained with TTC. (B) Correlation between infarct size measured using small-animal PET and TTC staining for given threshold in analysis of PET data (threshold = 60%). Correlation coefficient $r^2 = 0.92$, $P < 0.001$.

Some limitations of the present study should be considered. First, although our results suggest that the current preclinical findings may be suitable in clinical studies (because of the stable uptake and excellent pharmacokinetics of ^{18}F-FPTP), our study was only an experimental study in rodent models. Further preclinical application is being addressed with a pig model that more closely resembles the human heart in its size, heart rate, myocardial blood flow, and mitochondrial density. Second, our study was limited to acute MI with permanent LCA ligation. This model was well suited to determine myocardial defects but is not identical to the clinical situation in which hemodynamically relevant stenosis is unmasked by a stress-induced increase of myocardial blood flow. Further studies are needed to validate ^{18}F-FPTP PET for the detection of small myocardial ischemia and scars of chronic infarctions. We are currently pursuing the measurement of LV systolic function in cardiac-gated ^{18}F-FPTP PET by comparing it with the MI size using rat models after permanent or transient LCA ligation.

CONCLUSION

The present study was performed to synthesize and evaluate the feasibility of ^{18}F-FPTP as a PET tracer for the assessment of myocardial abnormalities.^{18}F-FPTP showed stable uptake in the myocardium and rapid clearance from the blood and other organs and enabled an excellent image quality and accurate evaluation of MI size in rat models of coronary occlusion. It may be a useful tool that allows the accurate and comprehensive evaluation of MI in preclinical trials and high throughput with multiple daily studies and a wide distribution of PET myocardial imaging in the clinic.

DISCLOSURE STATEMENT

The costs of publication of this article were defrayed in part by the payment of page charges. Therefore, and solely to indicate this fact, this article is hereby marked "advertisement" in accordance with 18 USC section 1734.

ACKNOWLEDGMENTS

We thank Seung Hyun Chong for his excellent research assistance. This research was supported by the National Research Foundation of Korea (NRF) (no. 2011-0029941) and by the Pioneer Research Center Program through the National Research Foundation of Korea (no. 2010-0002241) funded by the Ministry of Education, Science and Technology. No other potential conflict of interest relevant to this article was reported.

REFERENCES

1. Camici PG, Rimoldi OE. The clinical value of myocardial blood flow measurement. *J Nucl Med.* 2009;50:1076–1087.
2. Madar I, Ravert HT, Du Y, et al. Characterization of uptake of the new PET imaging compound ^{18}F-fluorobenzyl triphenyl phosphonium in dog myocardium. *J Nucl Med.* 2006;47:1359–1366.
3. Knuuti J, Bengel FM. Positron emission tomography and molecular imaging. *Heart.* 2008;94:360–367.
4. Siegrist PT, Husmann L, Knabenhans M, et al. ^{13}N-ammonia myocardial perfusion imaging with a PET/CT scanner: impact on clinical decision making and cost-effectiveness. *Eur J Nucl Med Mol Imaging.* 2008;35: 889–895.
5. Sampson UK, Dorbala S, Limaye A, Kwong R, Di Carli MF. Diagnostic accuracy of rubidium-82 myocardial perfusion imaging with hybrid positron emission tomography/computed tomography in the detection of coronary artery disease. *J Am Coll Cardiol.* 2007;49:1052–1058.
6. Huisman MC, Higuchi T, Reder S, et al. Initial characterization of an ^{18}F-labeled myocardial perfusion tracer. *J Nucl Med.* 2008;49:630–636.
7. Yu M, Guaraldi MT, Mistry M, et al. BMS-747158-02: a novel PET myocardial perfusion imaging agent. *J Nucl Cardiol.* 2007;14:789–798.
8. Kim DY, Kim HJ, Yu KH, Min JJ. Synthesis of [^{18}F]-labeled (6-fluorohexyl) triphenylphosphonium cation as a potential agent for myocardial imaging using positron emission tomography. *Bioconjug Chem.* 2012;23:431–437.
9. Kim DY, Kim HJ, Yu KH, Min JJ. Synthesis of [^{18}F]-labeled (2-(2-fluoroethoxy)ethyl)triphenylphosphonium cation as a potential agent for myocardial imaging using positron emission tomography. *Bioorg Med Chem Lett.* 2012; 22:319–322.
10. Madar I, Ravert H, Nelkin B, et al. Characterization of membrane potential-dependent uptake of the novel PET tracer ^{18}F-fluorobenzyl triphenylphosphonium cation. *Eur J Nucl Med Mol Imaging.* 2007;34:2057–2065.
11. Kim DY, Yu KH, Bom HS, Min JJ. Synthesis of (4-[^{18}F]fluorophenyl)triphenylphosphonium as a mitochondrial voltage sensor for PET. *Nucl Med Mol Imaging.* 2007;41:561–565.
12. Zhen Cheng MS. Xiaoyuan Chen, Sanjiv Sam Gambhir. Synthesis of (4-[^{18}F]fluorophenyl)triphenylphosphonium as a potential imaging agent for mitochondrial dysfunction. *J Labelled Compd Radiopharm.* 2005;48:131–137.
13. Min JJ, Biswal S, Deroose C, Gambhir SS. Tetraphenylphosphonium as a novel molecular probe for imaging tumors. *J Nucl Med.* 2004;45:636–643.
14. Madar I, Ravert H, Dipaula A, Du Y, Dannals RF, Becker L. Assessment of severity of coronary artery stenosis in a canine model using the PET agent ^{18}F-fluorobenzyl triphenyl phosphonium: comparison with ^{99m}Tc-tetrofosmin. *J Nucl Med.* 2007;48:1021–1030.
15. Murphy MP. Selective targeting of bioactive compounds to mitochondria. *Trends Biotechnol.* 1997;15:326–330.
16. Fukuda H, Syrota A, Charbonneau P, et al. Use of ^{11}C-triphenylmethylphosphonium for the evaluation of membrane potential in the heart by positron-emission tomography. *Eur J Nucl Med.* 1986;11:478–483.
17. Higuchi T, Fukushima K, Rischpler C, et al. Stable delineation of the ischemic area by the PET perfusion tracer ^{18}F-fluorobenzyl triphenyl phosphonium after transient coronary occlusion. *J Nucl Med.* 2011;52:965–969.
18. Kroemer G. Mitochondrial control of apoptosis: an introduction. *Biochem Biophys Res Commun.* 2003;304:433–435.
19. Ross MF, Kelso GF, Blaikie FH, et al. Lipophilic triphenylphosphonium cations as tools in mitochondrial bioenergetics and free radical biology. *Biochemistry (Mosc).* 2005;70:222–230.
20. Cesselli D, Jakoniuk I, Barlucchi L, et al. Oxidative stress-mediated cardiac cell death is a major determinant of ventricular dysfunction and failure in dog dilated cardiomyopathy. *Circ Res.* 2001;89:279–286.
21. Yu KH, Kim YS, Kim SW, et al. Synthesis of [^{18}F]Fluoroclofilium as a potential cardiac imaging agent for PET studies. *J Labelled Compd Radiopharm.* 2003;46: 1151–1160.
22. Ravert HT, Madar I, Dannals RF. Radiosynthesis of 3-[^{18}F]fluoropropyl and 4-[^{18}F]fluorobenzyl triarylphosphonium ions. *J Labelled Compd Radiopharm.* 2004; 47:469–476.
23. Zhou Y, Liu S. ^{64}Cu-labeled phosphonium cations as PET radiotracers for tumor imaging. *Bioconjug Chem.* 2011;22:1459–1472.
24. Kim YS, Yang CT, Wang J, et al. Effects of targeting moiety, linker, bifunctional chelator, and molecular charge on biological properties of ^{64}Cu-labeled triphenylphosphonium cations. *J Med Chem.* 2008;51:2971–2984.
25. Sachin K, Kim EM, Cheong SJ, et al. Synthesis of N'-[^{18}F]fluoroalkylated ciprofloxacin as a potential bacterial infection imaging agent for PET study. *Bioconjug Chem.* 2010;21:2282–2288.
26. Steen H, Maring JG, Meijer DK. Differential effects of metabolic inhibitors on cellular and mitochondrial uptake of organic cations in rat liver. *Biochem Pharmacol.* 1993;45:809–818.
27. Cheng Z, Winant RC, Gambhir SS. A new strategy to screen molecular imaging probe uptake in cell culture without radiolabeling using matrix-assisted laser desorption/ionization time-of-flight mass spectrometry. *J Nucl Med.* 2005;46: 878–886.
28. Samsamshariat SA, Samsamshariat ZA, Movahed MR. A novel method for safe and accurate left anterior descending coronary artery ligation for research in rats. *Cardiovasc Revasc Med.* 2005;6:121–123.
29. *Guide for the Care and Use of Laboratory Animals*. Bethesda, MD: National Institutes of Health; 1985. NIH publication 85–23.
30. Schepis T, Gaemperli O, Treyer V, et al. Absolute quantification of myocardial blood flow with ^{13}N-ammonia and 3-dimensional PET. *J Nucl Med.* 2007;48: 1783–1789.
31. Koepfli P, Hany TF, Wyss CA, et al. CT attenuation correction for myocardial perfusion quantification using a PET/CT hybrid scanner. *J Nucl Med.* 2004;45: 537–542.
32. Acton PD, Thomas D, Zhou R. Quantitative imaging of myocardial infarct in rats with high resolution pinhole SPECT. *Int J Cardiovasc Imaging.* 2006;22: 429–434.
33. Gibbons RJ, Valeti US, Araoz PA, Jaffe AS. The quantification of infarct size. *J Am Coll Cardiol.* 2004;44:1533–1542.
34. Grinius LL, Jasaitis AA, Kadziauskas YP, et al. Conversion of biomembrane-produced energy into electric form. I. Submitochondrial particles. *Biochim Biophys Acta.* 1970;216:1–12.
35. Nakajima K, Taki J, Shuke N, Bunko H, Takata S, Hisada K. Myocardial perfusion imaging and dynamic analysis with technetium-99m tetrofosmin. *J Nucl Med.* 1993;34:1478–1484.
36. Okada RD, Glover D, Gaffney T, Williams S. Myocardial kinetics of technetium-99m-hexakis-2-methoxy-2-methylpropyl-isonitrile. *Circulation.* 1988;77:491–498.
37. Nuyts J, Dupont P, Van den Maegdenbergh V, Vleugels S, Suetens P, Mortelmans L. A study of the liver-heart artifact in emission tomography. *J Nucl Med.* 1995;36: 133–139.
38. Kailasnath P, Sinusas AJ. Comparison of Tl-201 with Tc-99m-labeled myocardial perfusion agents: technical, physiologic, and clinical issues. *J Nucl Cardiol.* 2001;8:482–498.